MID-AMERICA TRANSPORTATION CENTER

Report # MATC-MST: 241

Final Report

Validation on the Mechanical Models of Asphalt Pavement Structures with Field Measured Data Associated with Increasing Freight Movements

Yu-Ning Ge, Ph.D.
Assistant Professor
Department of Civil, Architectural, and Environmental Engineering
Missouri University of Science and Technology

Genda Chen, P.E., Ph.D.

2011

A Cooperative Research Project sponsored by the U.S. Department of Transportation Research and Innovative Technology Administration

Validation on the Mechanical Models of Asphalt Pavement Structures with Field Measured Data Associated with Increasing Freight Movements

Dr. Yu-Ning Ge
Department of Civil, Architectural, and
Environmental Engineering
Missouri University of Science and Technology

Dr. Genda Chen
Department of Civil, Architectural, and
Environmental Engineering
Missouri University of Science and Technology

A Report on Research Sponsored by

Mid-America Transportation Center
2200 Vine Street
PO Box 830851
Lincoln, NE 68583-0851

October 5, 2011

Technical Report Documentation Page

1. Report No. 25-1121-0001-241	2. Government Accession No.	3. Recipient's Catalog No.
4. Title and Subtitle Validation on the Mechanical Models of Asphalt Pavement Structures with Field Measured Data Associated with Increasing Freight Movements		5. Report Date October 5, 2011 6. Performing Organization Code
7. Author(s) Dr. Yu-Ning Ge and Dr. Genda Chen		8. Performing Organization Report No. **25-1121-0001-241**
9. Performing Organization Name and Address Mid-America Transportation Center 2200 Vine St. PO Box 830851 Lincoln, NE 68583-0851		10. Work Unit No. (TRAIS) 11. Contract or Grant No.
12. Sponsoring Agency Name and Address Research and Innovative Technology Administration 1200 New Jersey Ave., SE Washington, D.C. 20590		13. Type of Report and Period Covered 14. Sponsoring Agency Code MATC TRB RiP No18470

15. Supplementary Notes

16. Abstract

This study is aimed at better understanding the effects of heavy trucks on the performance of asphalt pavements. As the U.S. freight movements are dominated by truck transportations, the addition of new roadway lane-miles in Region VII have not kept pace with the increase in truck volume. As such, existing highway pavements must be effectively preserved under heavy truck loads. The key to the success of infrastructure preservation is to accurately predict the behavior of pavement structures. To this end, it was necessary for the study to collect sufficient field performance data.

The data were used to validate the Mechanistic Empirical Pavement Design Guide (MEPDG) and the finite element method (FEM), in terms of the impact of heavy truck loading on pavement performance. Actual roadway sections in Missouri were selected and monitored several times over the project period. Pavement performance-related data such as traffic information, asphalt material properties, and subgrade condition were collected and used for various analyses. The study provides insights into effective implementation of the MEPDG into the design and analysis of pavements in Region VII. The study's findings provide necessary information for the development of the next generation of a rigorously mechanics-based MEPDG. The outcome of the study led to better understanding of the pavement structure designs; which can result in long lasting transportation infrastructure and improve public safety. The study was completed in close coordination with Professor Yong-Rak Kim from the University of Nebraska-Lincoln through a parallel study that was separately proposed by Dr. Kim.

17. Key Words	18. Distribution Statement		
19. Security Classif. (of this report) Unclassified	20. Security Classif. (of this page) Unclassified	21. No. of Pages 46	22. Price

Table of Contents

List of Figures

List of Tables

Abstract

This study is aimed at better understanding the effects of heavy trucks on the performance of asphalt pavements. As the U.S. freight movements are dominated by truck transportations, the addition of new roadway lane-miles in Region VII have not kept pace with the increase in truck volume. As such, existing highway pavements must be effectively preserved under heavy truck loads. The key to the success of infrastructure preservation is to accurately predict the behavior of pavement structures. To this end, it was necessary for the study to collect sufficient field performance data.

The data were used to validate the Mechanistic Empirical Pavement Design Guide (MEPDG) and the finite element method (FEM), in terms of the impact of heavy truck loading on pavement performance. Actual roadway sections in Missouri were selected and monitored several times over the project period. Pavement performance-related data such as traffic information, asphalt material properties, and subgrade condition were collected and used for various analyses. The study provides insights into effective implementation of the MEPDG into the design and analysis of pavements in Region VII. The study's findings provide necessary information for the development of the next generation of a rigorously mechanics-based MEPDG. The outcome of the study led to better understanding of the pavement structure designs; which can result in long lasting transportation infrastructure and improve public safety. The study was completed in close coordination with Professor Yong-Rak Kim from the University of Nebraska-Lincoln through a parallel study that was separately proposed by Dr. Kim.

Executive Summary

Trucking is a key component of U.S. freight transportation. Trucks moved 71% of the total tonnage and 80% of the total value of U.S. shipments in 1998. By 2020, the U.S. transportation system is expected to handle about 23 billion tons of cargo valued at nearly $30 trillion. Freight shipment data has shown that freight either originates or terminates its journey in Nebraska and Missouri. Trucks moved a large percentage of the tonnage and value of these shipments and this is expected to grow, throughout the states, over the next ten years. Yet, even the significant addition of new lane-miles is not expected to keep pace with the increased demand for freight transportation. Therefore, the need to preserve existing highway infrastructure and to accomplish an appropriate design-analysis for new pavements must be a high priority.

This report consists of three parts. The first chapter presents a cyclic constitutive model that is capable of modeling material behaviors under repeated load. The cyclic fuzzy set model provides analytical and simple geometrical interpretation to formulate hardening, hysteresis features, materials memory, and kinematic mechanisms without relying upon complex analytical formulations. In addition, the cyclic fuzzy set model accounts for realistic stress-strain behavior under repeated load cycles, nonlinear dilatancy behavior, critical state soil mechanics concepts, and non-proportional loading.

The second chapter demonstrates the results of the proposed cyclic plasticity model for modeling the permanent deformation behavior under repeated load cycles. The resilient modulus can also be calculated from the stress-strain response from the fuzzy set plasticity model. The model is capable of mimicking the behaviors of unbound granular materials under repeated loads; which include reversal loading, nonlinear dilatancy, material memory, and long term behavior,

such as elastic shakedown. The elastic shakedown is achieved by controlling the material memory and plastic modulus parameters. It is particularly attractive for finite element analysis since a more realistic stress-strain response is available.

Lastly, chapter three discusses the use of the numerical optimization technique to calibrate a constitutive model. The modified Cam-Clay model was calibrated against the laboratory test data. Although the least-square type of objective function Case C is preferred, all of the proposed objective functions worked effectively. Up to four variables were calibrated using the Case-C objective function and the upper and lower bounds of these variables need to be specified. The efficiency of the optimization relies on the determination of the bound values.

Chapter 1 Cyclic Plasticity Constitutive Model

1.1 Introduction

In recent decades, the development of constitutive models for a wide range of engineering materials, including soils, has increased significantly (e.g., Prevost, 1978; Mroz et al., 1978; Sture et al., 1982; Vermeer, 1982; Bardet, 1985; Anandarajah, 1994; Muir Wood et al., 1994; Manzari and Dafalias, 1997; Gajo and Muir Wood, 1999). The majority of the models are based on incremental or flow plasticity theory. Due to the rapid expansion in the use of general-purpose geotechnical software among practicing engineers, nonlinear numerical analysis has become increasingly popular. These developments, along with elaborate color-graphic output schemes and user-friendly interface, give an unusual sense of confidence among users. Thus, it is important to develop reliable and versatile nonlinear soil models.

Within the framework of classical plasticity theory, isotropic hardening is sufficient to simulate the stress-strain behavior of soil under monotonic loading. Kinematic hardening or mixed hardening (isotropic and kinematic hardening) is typically used to mimic hysteretic phenomena of soil under cyclic loading, such as reverse plastic flow and memory of particular loading events. However, kinematic hardening models are complicated and often very difficult to implement in constitutive drivers within reliable finite element codes. Also, many of these models were designed and validated for specific stress paths, for example, conventional triaxial compression. They were not validated for or made useful for other loading paths, which clearly take place in general boundary value problems of geotechnical engineering and structure-soil interaction. This chapter presents a cyclic constitutive model based on fuzzy set plasticity capable of describing repeated load cycles, dilatancy, material memory, drained and undrained

behavior, features of critical state soil mechanics, density and mean effective stress dependence, and long-term cyclic effects (elastic shakedown).

1.2 Cyclic Fuzzy Set Plasticity Model Formulation

The concept of fuzzy set plasticity was first introduced by Klisinski et al. (1988) and its theory and formulation has since been described by several researchers. Unlike conventional elasto-plastic hardening models, the fuzzy set model is physically intuitive and easy to visualize. It provides analytical and simple geometrical interpretation to formulate hardening, hysteresis features, material memory, and kinematic mechanisms without using complicated kinematic hardening formulations.

1.2.1 Elastic Behavior

The bulk modulus K and shear modulus G are pressure dependent parameters defined as

$$K = \frac{(1+e)}{\kappa} p' \tag{1.1}$$

$$G = \frac{3(1-2\nu)}{2(1+\nu)} K \tag{1.2}$$

,

where,

e is the void ratio, ν is the Poisson's ratio, and κ is the slope of the unloading-reloading line on e versus log p' curve.

1.2.2 Membership Function

The membership function has been involved in the plastic modulus equations. When $\gamma = 1$, the material behaves purely elastically and the corresponding value of the plastic modulus

is infinite. However, when $\gamma = 0$, the material reaches a fully plastic state and the plastic modulus is equal to the value on the fuzzy surface, i.e. $H = H^*$.

With the assistance of the membership function γ, we can readily construct reversal plastic loading without resorting to a kinematic hardening rule. The following are the basic rules of kinematic mechanism for the membership functions: for plastic loading and plastic unloading, $\dot{\gamma} < 0$; and for elastic loading and elastic unloading, $\dot{\gamma} \geq 0$. Although the value of the membership function is 1 at a fully elastic state and 0 at the fully plastic state, the assignment of the value in elastoplastic state is deterministic and can be arbitrarily defined as needed. A linear variation with respect to stress state was adopted in this study.

The kinematic mechanism of the membership function γ is shown in figure 1.1, which represents plastic loading from point *a* to *b*, followed by elastic unloading from point *b* to *c*. After point *c* is reached, unloading with the associated decrease of the value of the membership function results in plastic deformation, which is a feature of the membership function. The degree of material memory can be simulated by predetermining the location of point *c*. Furthermore, by controlling the location of point *c*, one can also model elastic shakedown behavior, where point *c* moves toward a point as cyclic loading proceeds. Plastic unloading, or reversal loading, is shown from point *c* to point *d*. This is followed by elastic loading from point *d* to point *e* and plastic loading from point *e* to point *b*, as shown in figure 1.1.

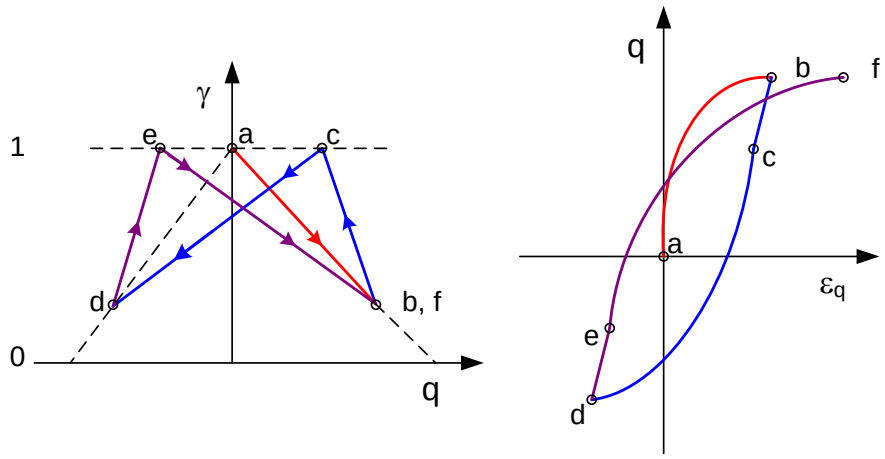

Figure 1.1 Illustration of kinematic mechanism of the membership function

Figure 1.2 displays an example of the deviatoric stress-strain response and evolution of the membership function for a material subjected to two varied amplitude cyclic loadings under a conventional triaxial stress path. The unloading and reloading points take place in two different stress levels, q = 156 kPa and q = 231 kPa, respectively. The two graphs on the left highlight cycle 1 with the loading from 0 to 156 kPa and unloading from 156 to 0 kPa (solid line). The two graphs on the right illustrate cycle 2 with the loading from 0 to 231 kPa and unloading from 231 to 0 kPa (solid line).

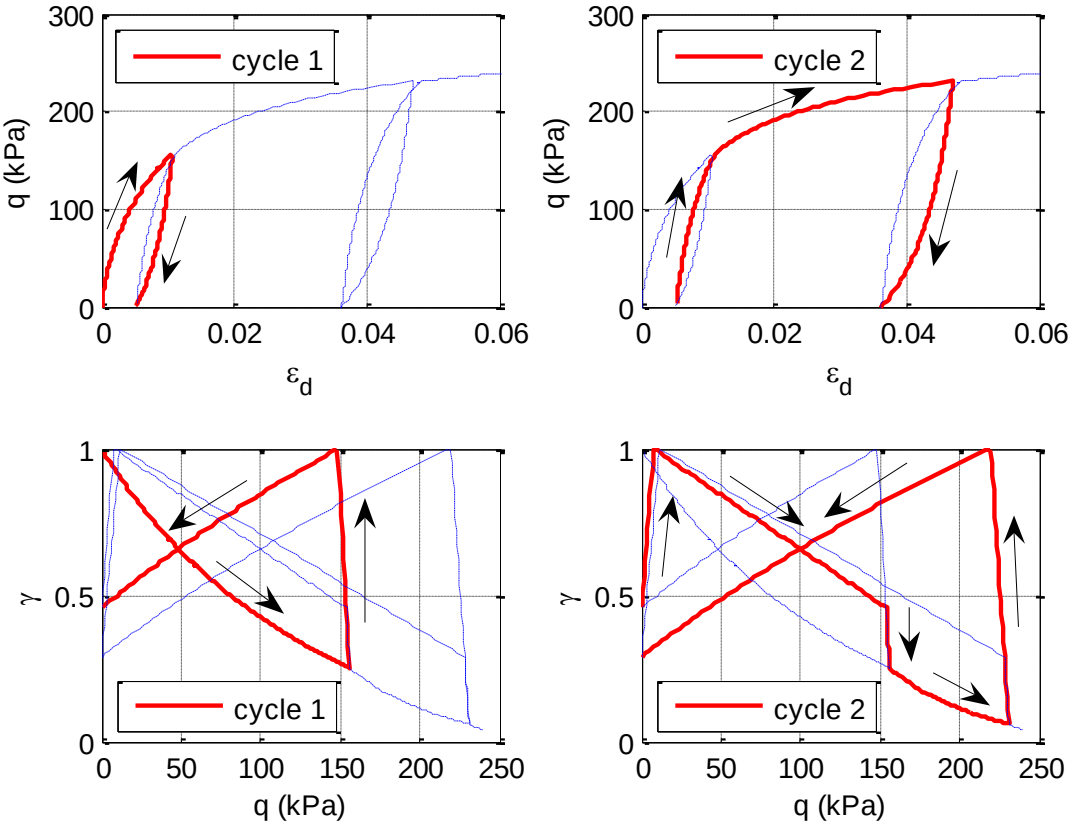

Figure 1.2 Deviatoric stress-strain curve and evolution of the membership function *g* for cycle 1 and cycle 2

1.2.3 Fuzzy surface

The fuzzy surface is a three-stress-invariant function which can be expressed as:

$$F^c = r - a_0 - a_1 p - a_2 p^2 = 0 \quad \text{in triaxial compression;} \tag{1.3}$$

$$F^e = r - b_0 - b_1 p - b_2 p^2 = 0 \quad \text{in triaxial extension;} \tag{1.4}$$

where

r and p are stress invariants.

These are defined below as

$$r = q \cdot g(\theta, \chi), \tag{1.5}$$

$$p = \frac{1}{3} I_1, \tag{1.6}$$

$$q = \sqrt{3J_2}\ . \tag{1.7}$$

The first stress invariant corresponding to mean stress is *p* and the second deviatoric stress invariant relating to shear stress is *q*. The elliptical function $g = g(\theta, \chi)$, proposed by Willam and Warnke (1974), is considered to be the third invariant in the fuzzy surface. It is a function of the Lode angle θ and the ellipticity χ, which controls the shape of fuzzy surface in deviatoric stress plane as shown in figure 1.3 below. Material constants, a_0, a_1, a_2, b_0, b_1, and b_2, can be determined from triaxial compression and extension tests. Also, the fuzzy surface can be curvilinear lines in the *p*-*q* stress space with non-zero values of a_2 and b_2. In this paper, a linear fuzzy surface was considered.

$$g(\theta, \chi) = \frac{4(1-\chi^2)\cos^2(\theta - \frac{\pi}{3}) + (2\chi - 1)^2}{2(1-\chi^2)\cos(\theta - \frac{\pi}{3}) + (2\chi - 1)[4(1-\chi^2)\cos^2(\theta - \frac{\pi}{3}) + 5\chi^2 - 4\chi]^{\frac{1}{2}}} \tag{1.8}$$

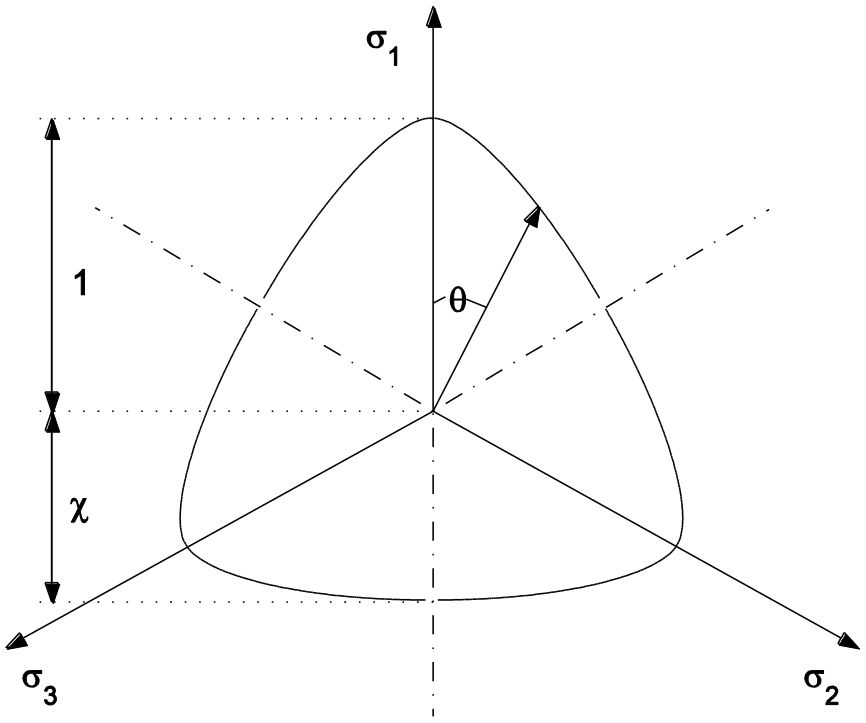

Figure 1.3 Willam-Warnke deviatoric contour

The stress-strain behavior under non-proportional loading, ranging from compression to extension, can be captured by varying the Lode angle. The ellipticity $\chi = \chi(p)$ can also be dependent on effective mean confining stress p, where it is anticipated that the deviatoric trace of the fuzzy surface will become almost circular for large values of the mean confining stress ($\chi = 1$). For low mean confining stress levels ($\chi = ½$), the trace degenerates to a triangle. The value of the elliptical function at each stress state can be calculated and the fuzzy surface can be described in the conventional triaxial p-q stress space.

The coefficient a_1 in the fuzzy surface function for triaxial compression incorporates the concept of critical state soil mechanics, which is defined as

$$a_1 = M_c + \kappa_s \langle -\psi \rangle, \tag{1.9}$$

where,

M_c is the stress ratio q/p at critical state, κ_s is a constant, and ψ is a *state parameter*, which is defined as the difference between the current void ratio e and the critical state void ratio.

For loose granular materials, $\psi > 0$ and $a_1 = M_c$, whereas dense granular materials, $\psi > 0$ and a_1 will evolve with the change of ψ during loading and finally reach critical state, $\psi = 0$ and $a_1 = M_c$. The evolution of state parameter $\dot{\psi}$ is derived from the void ratio versus log mean stress plot,

$$\dot{\psi} = -(1 + e_0)\dot{\varepsilon}_v^p + \frac{C_\lambda}{p}\dot{p} \tag{1.10}$$

where,

C_λ is the slope of the critical line in void ratio versus log mean stress plot.

1.2.4 Plastic Modulus

Since the loading surface is not explicitly defined in the fuzzy set plasticity model, one can think that for the current stress state, there exists a loading surface such that the plastic modulus is defined as follows.

$$H = H^* + \frac{M\gamma^d}{1-\gamma^{d+1}} \tag{1.11}$$

where,

d and *M* are model parameters that can be determined from test data.

1.2.5 Flow Rules

Plastic flow rules are expressed as $\dot{\boldsymbol{\varepsilon}}^p = \dot{\lambda}\mathbf{m}$, where **m** is the direction of plastic deformation increments. In classic plasticity theory, the plastic potential is required to determine the direction of the plastic deformation increment. In the fuzzy set plasticity theory, a fourth-order tensor is defined in such a way that **m** = **T** : **n**, where T is a fourth-order tensor. If **T** = **I**, we have associated plastic flow. Therefore, the effect of non-associated flow rules is achieved by defining a fourth-order tensor **T** so that the plastic potential function need not be known explicitly. This fourth-order tensor **T** is defined as:

$$\mathbf{T} = \mathbf{I} - \frac{1}{3}(1-D)\mathbf{1}\otimes\mathbf{1}\,, \tag{1.12}$$

where,

D is called dilatancy parameter and can be expressed as $D = A[a_1 B - \eta]$ in triaxial compression, and $D = A[b_1 B - \eta]$ in triaxial extension in the current model.

The parameters from fuzzy surface equations are a_1 and b_1, and η is the current stress ratio q/p. The matrix form of **T** is expressed as a 6×6 matrix in a triaxial stress space, which can be reduced to a 2×2 matrix in the conventional triaxial p-q spaceas follows,

$$T = \begin{bmatrix} \frac{1}{3}(D+2) & \frac{1}{3}(D-1) & \frac{1}{3}(D-1) & 0 & 0 & 0 \\ \frac{1}{3}(D-1) & \frac{1}{3}(D+2) & \frac{1}{3}(D-1) & 0 & 0 & 0 \\ \frac{1}{3}(D-1) & \frac{1}{3}(D-1) & \frac{1}{3}(D+2) & 0 & 0 & 0 \\ 0 & 0 & 0 & 1 & 0 & 0 \\ 0 & 0 & 0 & 0 & 1 & 0 \\ 0 & 0 & 0 & 0 & 0 & 1 \end{bmatrix} \tag{1.13}$$

$$T = \begin{bmatrix} D & 0 \\ 0 & 1 \end{bmatrix}. \tag{1.14}$$

1.3 Model Validation

The cyclic triaxial tests on Fuji sand (Pradhan et al. 1989) and Toyoura sand (Tatsuoka and Ishihara 1974) were used to calibrate and validate the cyclic fuzzy set model. For the Fuji sand, the material parameters used were:

$\kappa = 0.001$, $\nu = 0.3$, $a_1 = 1.48$, $b_1 = -1.08$, $\chi = 0.73$, $M = 10450$, $d = 2.48$, $a_0 = 0$, $b_0 = 0$, $A = 0.17$, and $B = 1.05$. (1.15)

The stress-strain response is given in figure 1.4. In general, the model captures the trend of the laboratory measurement quite well for the first three cycles under lower stress amplitude.

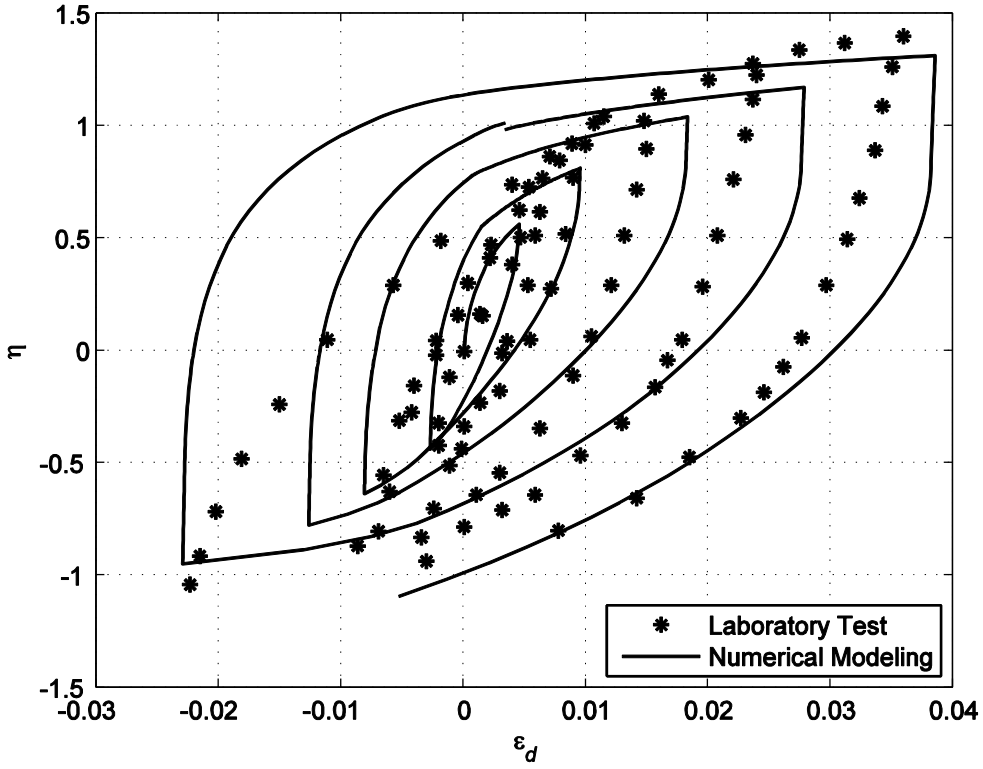

Figure 1.4 Stress ratio versus deviatoric strain response for Fuji sand

On the other hand, it is obvious that the model does not match the stress-strain curves under higher stress amplitude (4th and 5th cycle). This is mainly due to that fact that the degradation of the plastic shear modulus was not taken into consideration. On the volumetric behavior, as shown in figure 1.5, the fuzzy set model response matches the laboratory measurement satisfactorily.

For the Toyoura sand, these were the model parameters used:

$\kappa = 0.001,\ \nu = 0.3,\ a_1 = 1.24,\ b_1 = -1.08,\ \chi = 0.87,\ M = 8450,\ d = 2.8,$

$a_0 = 0,\ b_0 = 0,\ A = 0.28,$ and $B = 1.05.$ (1.16)

Figures 1.6 and 1.7 show the deviatoric and volumetric behaviors under cyclic triaxial, respectively. Similar observations and conclusions drawn from Fuji sand can also be applied to Toyoura sand.

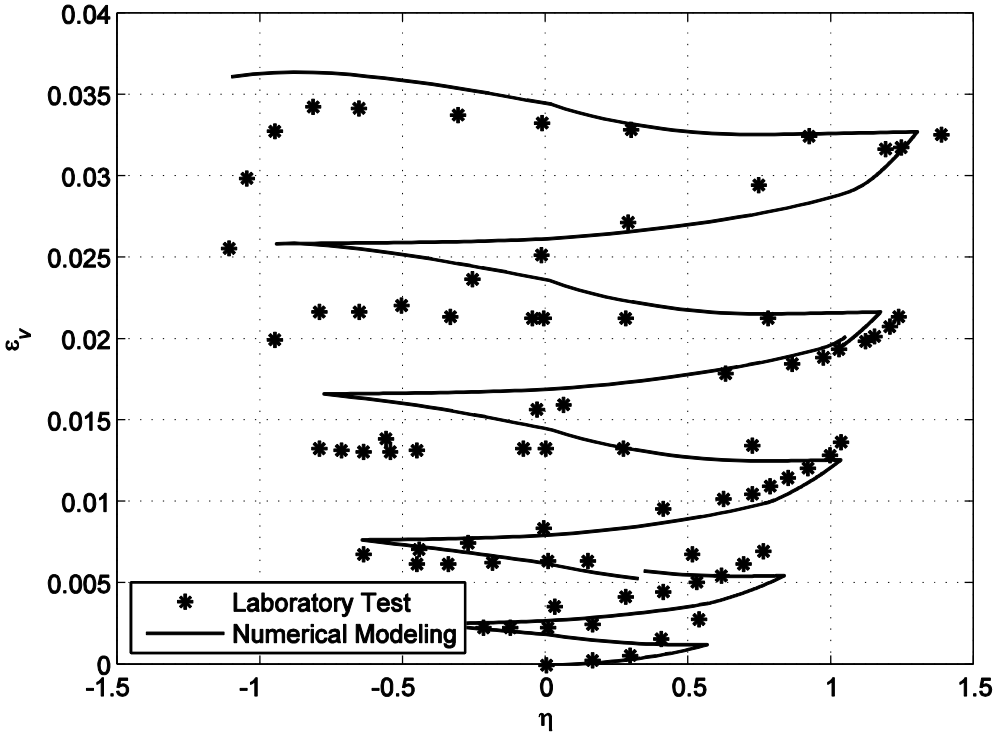

Figure 1.5 Volumetric strain versus stress ratio response for Fuji sand

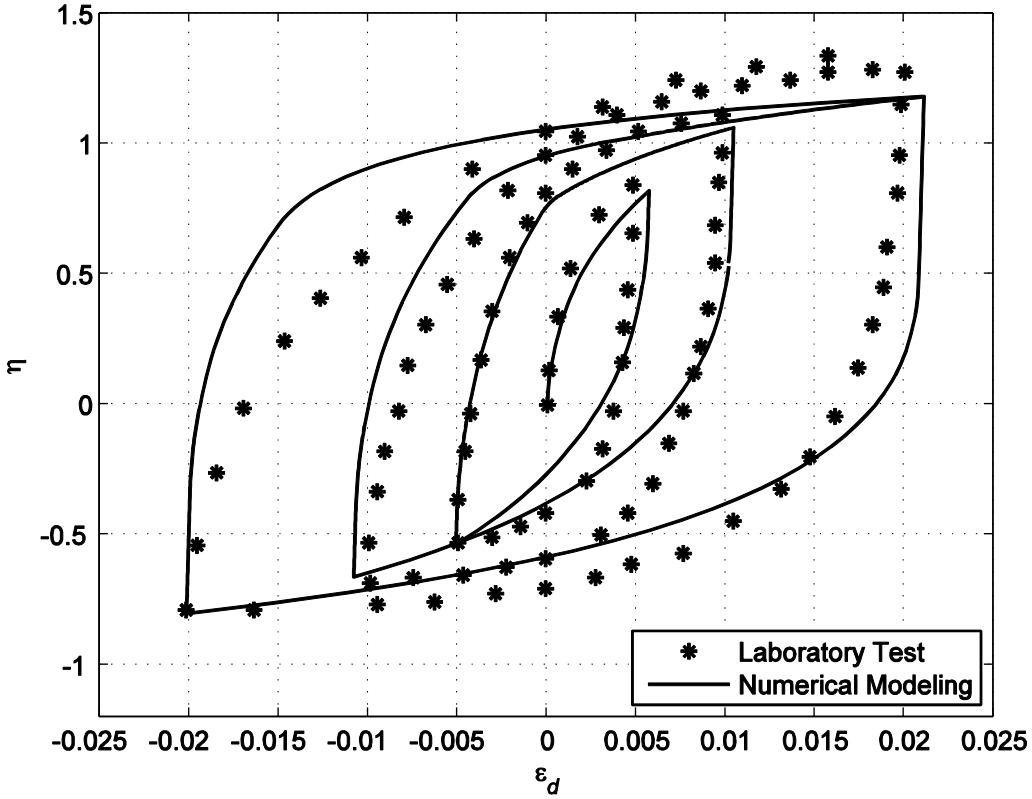

Figure 1.6 Stress ratio versus deviatoric strain response for Toyoura sand

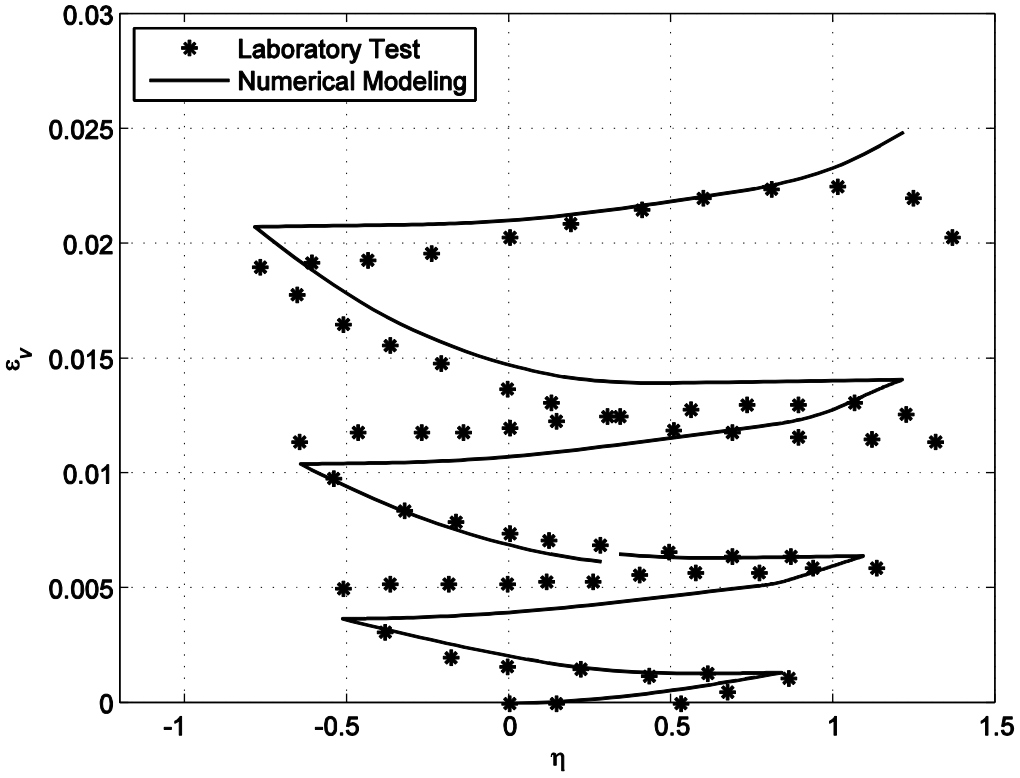

Figure 1.7 Volumetric strain versus stress ratio response for Toyoura sand

1.4 Summary

A cyclic constitutive model based on fuzzy set concepts has been developed. The cyclic fuzzy set model is physically intuitive and easy to visualize with the aid of membership functions. The cyclic fuzzy set model provides analytical and simple geometrical interpretation to formulate hardening, hysteresis features, materials memory, and kinematic mechanisms without relying upon complex analytical formulations. In addition, the cyclic fuzzy set model accounts for realistic stress-strain behavior under repeated load cycles, nonlinear dilatancy behavior, critical state soil mechanics concepts, and non-proportional loading. The evolution rule for the fuzzy surface can help simulate the post peak soil behavior such as strain softening. The

critical state soil mechanics concept has been implemented into the fuzzy set model by linking the fuzzy surface parameter a_1 to the state parameter ψ.

Chapter 2 Modeling Permanent Deformation of Pavement Base Materials

2.1 Introduction

Permanent deformation is one of the important factors used to evaluate the performance of a pavement structure under a service load. Depending upon the stress history on pavement due to a moving wheel load, the accumulated permanent deformation could keep increasing with continued load cycles or reach a stabilized value which is called elastic shakedown (Werkmeister et al. 2004; Garcia-Rojo and Herrmann 2005). For moderate stress levels, elastic shakedown is expected when the material response is typically characterized by the resilient elastic modulus after numerous cycles. It is preferred so that the life of the pavement lasts longer. Through laboratory and field measurements and observations, empirical equations have been widely used in predicting permanent deformation under repeated load (Lekarp et al. 2000a). Empirical equations are simple to use for practical design; however, they normally lack a physical framework to be formulated and a well-defined stress-strain relationship. Because of those reasons, finite element analysis has been popular in analyzing and modeling a pavement structure under traffic load.

In order to carry out an accurate analysis, a constitutive model capable of describing material behaviors under repeated loading is desired. Most of the constitutive models used in finite element analysis for pavement structures are non-linear elastic models defined by empirical resilient modulus equations (Lekarp et al. 2000b; Kim and Tutumluer 2008). Few isotropic/kinematic hardening elastoplastic models were used (e.g. Chazallon et al. 2006; Johnson and Sukumaran 2009) because applying thousands of repeated load cycles became computationally expensive. A majority of the models for granular materials are based on classic plasticity theory, where kinematic hardening or mixed hardening (isotropic and kinematic

hardening) is normally used to mimic hysteretic phenomena, such as reverse plastic flow and memory of particular loading events. However, they are sophisticated and often difficult to implement in constitutive drivers within reliable finite element codes.

Multi-surface plasticity, bounding surface plasticity, and generalized plasticity theories have been successfully used to model cyclic behavior of granular materials. In multi-surface plasticity (e.g. Prévost 1982), multiple yield surfaces take the shape of nested subspaces in stress space, where the stress-strain behavior within the innermost surface is assumed to be elastic. The instantaneous configuration of the field of yield surfaces was established by computing the parameters and equations that govern the translation, expansion, or contraction of individual surfaces during proportional, as well as non-proportional, loading and unloading. In bounding surface plasticity (e.g. Manzari and Dafalias 1997), the plastic strain occurs for stress states within the bounding surface. It is also possible to have a very flexible and smooth variation of the plastic modulus during straining, unlike the multi-surface plasticity model which assumes piecewise constant plastic moduli. As for generalized plasticity (e.g. Pastor and Zienkicwcz 1986), both plastic flow direction and plastic modulus for loading and unloading are defined explicitly where dilatancy was approximated by a linear function of stress invariant ratio as proposed by Nova and Wood (1979).

A cyclic plasticity model based on fuzzy set plasticity theory is presented in this paper to model the accumulated permanent axial strain and shakedown behavior of unbound granular materials under repeated loads. The concept of the fuzzy set plasticity was first introduced by Klisinski et al. (1988) and its theory and formulation have been described by several researchers (e.g. Klisinski 1991; Klisinski et al. 1991; Arduino and Macari 2001; Ge and Sture 2003a; 2003b). The model presented in this paper is capable of simulating realistic stress-strain

behaviors under repeated load cycles including nonlinear dilatancy, material memory, accurate reverse loading feature, non-proportional loading, and long-term cyclic effects. In the following sections, the framework of the fuzzy set plasticity theory is first introduced, followed by its model formulation, calibration, and performance.

2.2 Model Formulation

2.2.1 Material Memory

The material memory parameter α represents the material degree of memory and it shows the evolution of elastic and plastic deviatoric behavior during the entire loading and unloading (reversal loading) process. For $\alpha = 0$, it represents the materials that have no memory and it shows fully elastic behavior during the entire unloading process. For $\alpha = 1$, it represents the materials that have the maximum degree of memory and it shows fully plastic behavior during the entire unloading process. In order to describe the evolution of elastic and plastic behavior of unbound granular materials under repeated loading, the material memory function is given as

$$\alpha = \alpha_0 (N_i)^{m_3} \quad \alpha = \alpha_0 \left(N_i\right)^{m_3} \tag{2.1}$$

where,

α_0 is the initial value of α, N_i is the nth number of load application, m_3 is aparameter controlling the evolution of material memory parameter with load cycles. Figure 2.1 shows the evolution of memory function parameter under different m_3.

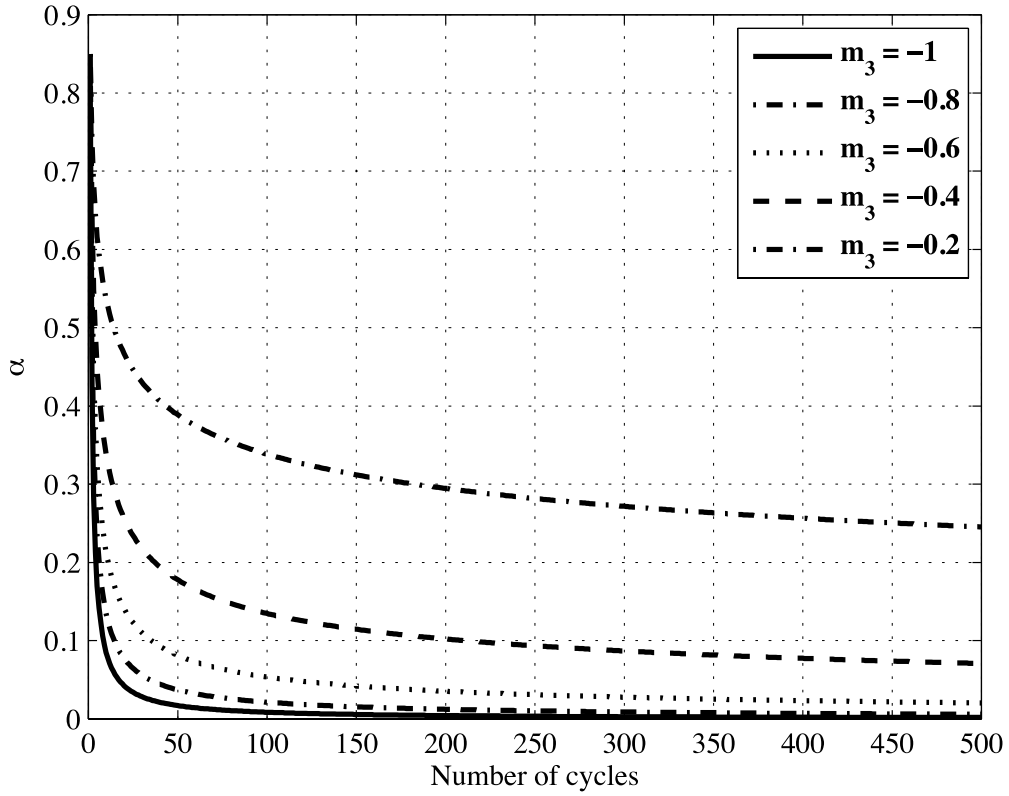

Figure 2.1 The evolution of material memory parameter α under different m_3

2.2.2 Flow Rules

The plastic strain increments follow the flow rules in classic plasticity theory,

$$\dot{\varepsilon}^{p} = \dot{\lambda}\mathrm{m}\,\dot{\boldsymbol{\varepsilon}}^{p} = \dot{\lambda}\mathbf{m} \tag{2.2}$$

where,

$\dot{\lambda}$ is the magnitude and ***m*** is the direction of the plastic strain increments.

In the fuzzy set plasticity, ***m*** is not determined through the gradient of plastic potential; instead, it is defined through a fourth tensor ***T***, for example

$$\mathrm{m} = \mathrm{T}:\mathrm{n}\,\mathbf{m} = \mathbf{T}:\mathbf{n} \tag{2.3}$$

In p-q space,

$$\mathbf{T} = \begin{bmatrix} D & 0 \\ 0 & 1 \end{bmatrix} \quad \mathrm{T} = \begin{bmatrix} \mathrm{D} & 0 \\ 0 & 1 \end{bmatrix} \quad \text{and}$$

$$\dot{\boldsymbol{\varepsilon}}^{p} = \begin{pmatrix} \dot{\varepsilon}_v^{p} \\ \dot{\varepsilon}_d^{p} \end{pmatrix} = \mathbf{T}:\mathbf{n} = \begin{bmatrix} D & 0 \\ 0 & 1 \end{bmatrix} \begin{pmatrix} \dfrac{\partial F_c}{\partial p} \\ \dfrac{\partial F_c}{\partial q} \end{pmatrix} \dot{\varepsilon}^{\mathrm{p}} = \begin{pmatrix} \dot{\varepsilon}_{\mathrm{v}}^{\mathrm{p}} \\ \dot{\varepsilon}_{\mathrm{d}}^{\mathrm{p}} \end{pmatrix} = \mathrm{T}:\mathrm{n} = \begin{bmatrix} \mathrm{D} & 0 \\ 0 & 1 \end{bmatrix} \begin{pmatrix} \mathrm{n_p} \\ \mathrm{n_q} \end{pmatrix}. \tag{2.4}$$

Shear-dilatancy incorporating current stress state η and critical state condition M_c is defined as,

$$\mathrm{D} = \frac{\partial \varepsilon_{\mathrm{v}}^{\mathrm{p}}}{\partial \varepsilon_{\mathrm{d}}^{\mathrm{p}}} = \mathrm{A}\left[\text{-}\mathrm{M_c}\kappa_{\mathrm{d}} + \eta\right] D = A\left(-M_c\kappa_d + \eta\right), \tag{2.5}$$

where,

A and κ_d are model parameter and η is the current stress ratio q/p.

In this paper, the evolution of the deviatoric plasticity modulus function parameter d is introduced as the following equation to account for the long term effects on the incremental plastic strain,

$$d = d_0\left[1 - m_1\left(\frac{N_i}{N_{cyc} - 1}\right)^{m_2}\right] \tag{2.6}$$

where,

N_{cyc} is the total number of load cycles, N_i is the number of current load cycles, m_1 and m_2 are exponential coefficients depending on the shear strain level, and d_0 is the initial values of the deviatoric plastic modulus function parameter. This can be used to simulate the elastic shakedown behavior when the material behaves elastically after certain amount of load cycles.

2.3 Model Calibration

With the advance of constitutive modeling, the parameters and constants required in elastoplastic models can be tremendous. Calibration of these constitutive models is not an easy task. In addition to the different types of laboratory experiments demanded, a systematic approach for model calibration is desired. Conventional method, such as linear regression, is not sufficient to identify the model parameters because many of them cannot be described in linear fashion through laboratory testing data. Moreover, some of these model parameters are defined with less physical meaning, which cause difficulties in model calibration. With this in mind, a numerical optimization technique of nonlinear least-square regression is applied to the constitutive model calibration. Optimization problems are generally defined as minimizing the objective function $f(\boldsymbol{x})$ subject to decision variable vector $\boldsymbol{x}$. Numerical optimization algorithms can be categorized into three groups according to the type of information needed to search for the minimum of the objective functions. The simplest way to minimize the objective function is to randomly choose a sufficiently large number of candidate vectors $\boldsymbol{x}$ and evaluate the objective function for each of them. In calibrating a fuzzy set plasticity model, the objective function is

defined by the Euclidean distance between an experimental point and a theoretical point and a random search method is used.

The random search method is considered to be the most inefficient but most easily implemented among the zero-order methods. For this reason, the random search method was adopted to calibrate the fuzzy set model in this paper. Moreover, the inefficiency can be overcome by the aid of modern high-speed computers. Assuming that the variables x^*_i for $i = 1$ to n lies between its lower bound x^l_i and upper bound x^u_i, there must exist a R_i such that $x^*_i = x^l_i + R_i(x^u_i - x^l_i)$ and minimize the objective function f.

Since constitutive models are being calibrated, it is intuitive to use stress and strain as variables in the objective function. It is then straightforward to formulate the objective function as the sum of distances from computed points to their adjacent experimental points in the stress strain space. For each computed strain that lies between $\varepsilon_j^{\exp}$ and $\varepsilon_{j+1}^{\exp}$, the distance between the computed and experimental strains can be calculated. The objective function is constructed as follows,

$$f = \sum_{i=1}^{n} \frac{1}{2}\left(\sqrt{\left(1-\frac{\sigma_j^{\exp}}{\sigma_i^{num}}\right)^2 + \left(1-\frac{\varepsilon_j^{\exp}}{\varepsilon_i^{num}}\right)^2} + \sqrt{\left(1-\frac{\sigma_{j+1}^{\exp}}{\sigma_i^{num}}\right)^2 + \left(1-\frac{\varepsilon_{j+1}^{\exp}}{\varepsilon_i^{num}}\right)^2} \right) \tag{2.7}$$

where,

n is the number of computed strains.

2.4 Model Performance

Three sets of laboratory experimental data from Lekarp (1997) were chosen to calibrate the fuzzy set plasticity model. Since the available lab data from Lekarp (1997) is not sufficient to calibrate the fuzzy set plasticity model and obtain a unique set of model parameters, appropriate assumptions were made to carry out the model calibration. The material types include Leighton Buzzard sand (S), sand and gravel (S&G), and slate waste (SW). The S&G and SW were tested in a triaxial cell apparatus, while the S was tested in a hollow cylinder apparatus. Lekarp's testing program was used with the primary aim of characterizing the development of cumulative permanent strain with number of load applications, as listed in table 2.1. The stress paths that were applied to the laboratory tests are also shown in table 2.1, where the corresponding load applications in p-q stress space were converted when the stress-strain responses were computed through the fuzzy set plasticity model. As Lekarp's tests available for model calibration are limited, the fuzzy set plasticity model parameters given in table 2.2 lead to one possible combination. Figure 2.3 shows the entire stress-strain curves for S under the stress paths listed in table 2.1. It was subjected to stress path P3 which shows more plastic deformation, as a higher maximum deviator stress (105 kPa) was applied. Both curves show the tendency of being more elastic as more load cycles are applied. Essentially, S under both stress paths P1 and P3 was stabilized and elastic shakedown was reached. The entire stress-strain behaviors for S&G and SW are similar so the curves are not shown in the paper.

Table 2.1 Selected tests from Lekarp (1997) for model calibration

Material	Stress path code	N (# of cycles)	σ_3 (kPa)		q (kPa)	
			min	max	min	max
S	P1	10000	70	70	0	80
	P3	10000	70	70	0	105
S&G	P1	10000	100	135	0	200
	P2	10000	100	285	0	500
	P3	10000	100	220	0	400
SW	P1	10000	0	20	0	300
	P2	10000	0	100	0	600
	P3	10000	0	200	0	600

Table 2.2 Fuzzy set plasticity model parameters

	K (MPa)	G (MPa)	M	d	a_0	a_1	A	κ_d	m_1	m_2	m_3	α
S-P1	580	700.9	105000	1.8	30	1.3	1.7	0.35	1.5	0.15	-0.62	0.85
S-P2	580	700.9	56000	1.8	30	1.3	1.7	0.35	1.5	0.21	-0.62	0.85
S&G-P1	580	700.9	405000	1.12	50	1.55	1.95	0.35	1.5	0.02	-0.62	0.85
S&G-P2	580	700.9	95000	1.8	50	1.55	1.95	0.35	1.5	0.46	-0.62	0.85
S&G-P3	580	700.9	50000	1.85	50	1.55	1.95	0.35	1.5	0.23	-0.62	0.85
SW-P1	580	700.9	572000	1.3	50	1.8	1.35	0.95	1.5	0.3	-0.62	0.85
SW-P2	580	700.9	572000	1.97	50	1.8	1.35	0.95	1.5	0.6	-0.62	0.85
SW-P3	580	700.9	793000	1.8	50	1.8	1.35	0.95	1.5	0.79	-0.62	0.85

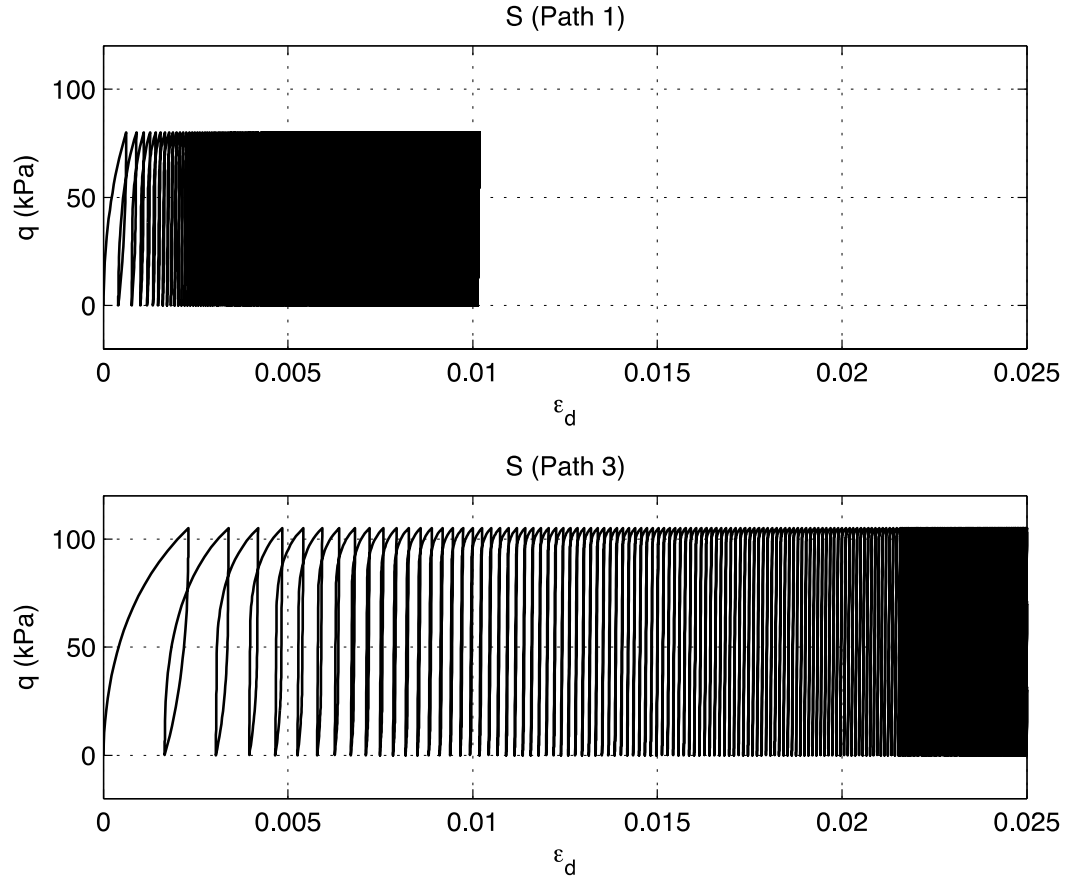

Figure 2.2 Complete stress-strain response for Leighton Buzzard sands

The permanent strain versus number of cycles curves for all three materials are presented in Figures 2.3, 2.4, and 2.5, respectively. It shows that the proposed cyclic plasticity model is capable of capturing the long term behavior in permanent deformation under repeated loads. In particular, most permanent axial strains were taking place in the first 2,000 load cycles. When the materials were subjected to higher deviatoric load repetitions, more load cycles were needed to reach a stable state (shakedown). As for resilient modulus, it can be calculated at any given load cycle since the entire stress-strain curve is available from the fuzzy set plasticity model.

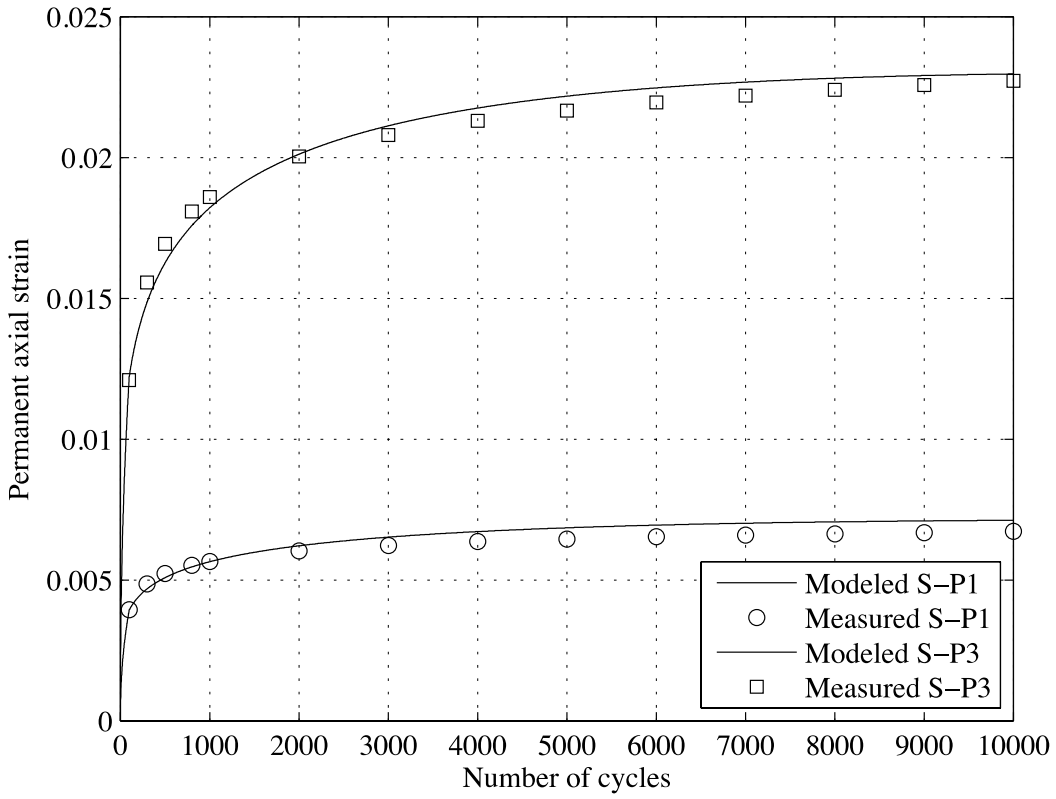

Figure 2.3 Permanent axial strain versus number of cycles for Leighton Buzzard sands

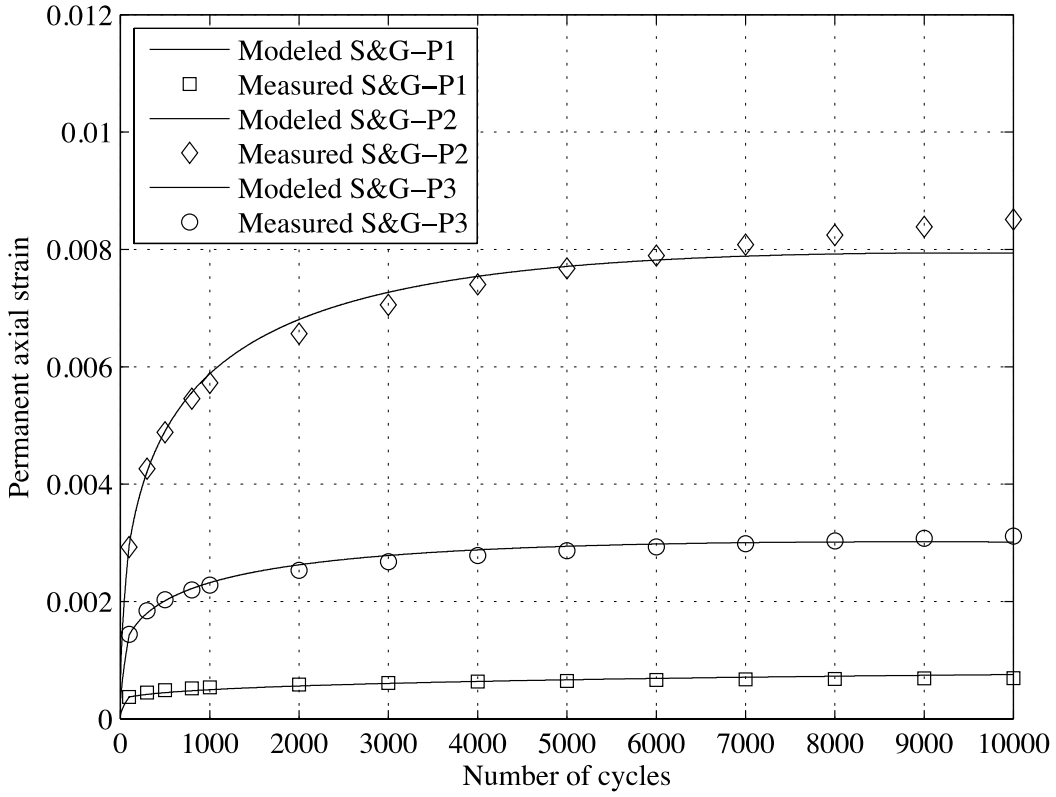

Figure 2.4 Permanent axial strain versus number of cycles for sand and gravel

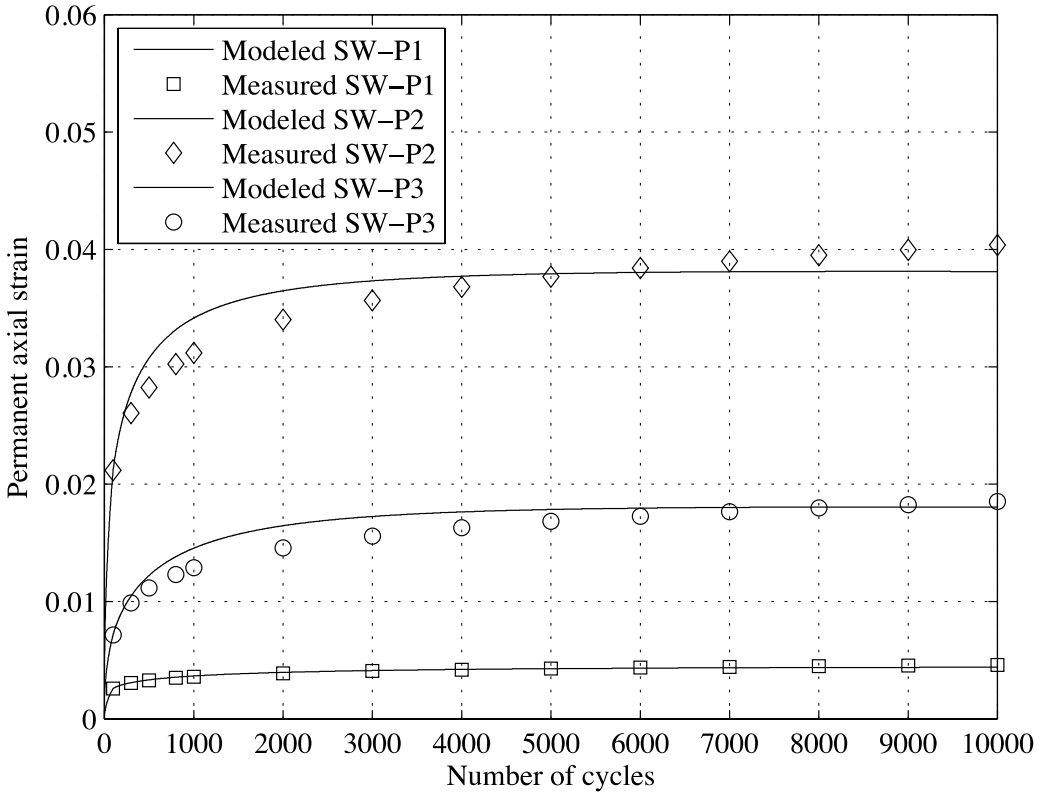

Figure 2.5 Permanent axial strain versus number of cycles for slate waste

Figure 2.6 shows an example of the calculated resilient modulus for S if a range of confining pressure is applied. Each resilient modulus was calculated from each corresponding stress-strain curve at its 10,000th cycle. It shows the trend that for a given maximum deviator stress, then the higher confinement and the higher the resilient modulus. It also shows that for a given confinement, then the higher maximum deviator stress and the higher the resilient modulus.

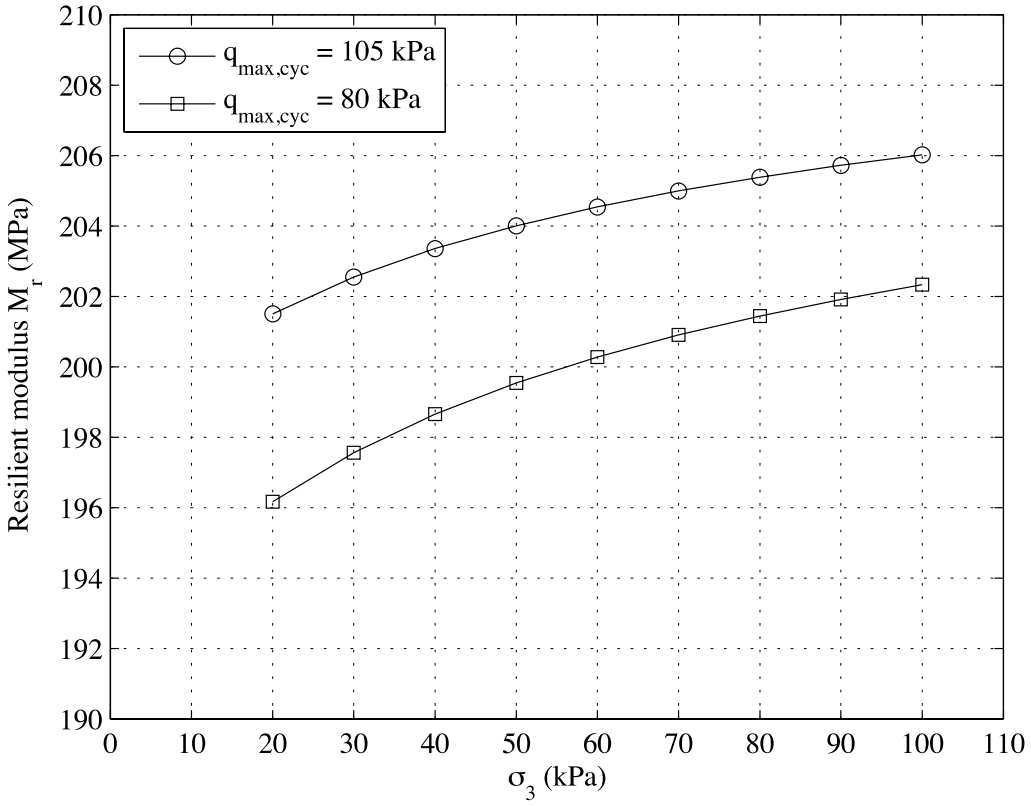

Figure 2.6 Calculated resilient modulus at various confining pressures for Leighton Buzzard sands

2.5 Summary

A cyclic plasticity model based on fuzzy set plasticity theory is presented in this paper for modeling the permanent deformation behavior under repeated load cycles. The resilient modulus can also be calculated from the stress-strain response from the fuzzy set plasticity model. The model is capable of mimicking the behaviors of unbound granular materials under repeated loads which include reversal loading, nonlinear dilatancy, material memory, and long term behavior such as elastic shakedown. The elastic shakedown is achieved by controlling the material memory and plastic modulus parameters. It is particularly attractive for finite element analysis

since a more realistic stress-strain response is available. However, it also has several drawbacks. Model calibration is challenging since it requires more laboratory test results. The triggering mechanisms for elastic shakedown, plastic shakedown, and progressive failure are not fully understood and not implemented into the model.

Chapter 3 Model Calibration Using Numerical Optimization Techniques

3.1 Introduction

With the advance of constitutive modeling, the parameters and constants required in elastoplastic models can be tremendous. Calibration of these constitutive models is not an easy task. In addition to the different types of laboratory experiments demanded, a systematic approach for model calibration is desired. Conventional method, such as linear regression, is not sufficient to identify the model parameters because many of them cannot be described in a linear fashion through laboratory testing data. Furthermore, some of these model parameters have less physical meaning, which causes difficulties in model calibration.

Several methods and algorithms have been developed and integrated for constitutive model calibration in recent decades. Mattsson et al. (2001) integrated the numerical optimization algorithms by Rosenbrock and the simplex method to calibrate an elastoplastic soil model. Johansson and Runesson (2002) used a function evaluation method to calibrate a plasticity model for granular materials, whereby a "multi-vector" strategy for choosing the appropriate start vector was proposed. Yang and Elgamal (2003) used three optimization methods: analytical, semi-analytical, and numerical, to calibrate a multi-surface plasticity sand model. Their calibration was based on the results from a number of drained triaxial tests and a dynamic centrifuge test. Calvello and Finno (2004) introduced an inverse analysis technique, which combines a finite element analysis and a parameter optimization algorithm, to calibrate an elastoplastic soil model. Johansson and Runnesson (2005) outlined a computational technique for constitutive model calibration with an automatic error control in space–time. Samarajiva et al. (2005) introduced a new fitness function, the objective function, to evaluate the fitness of material parameters based on stress and strain invariants using genetic algorithm. Cekerevac et

al. (2006) employed an optimization routine, which combines the quasi-Newton and stochastic methods, to calibrate an elastoplastic constitutive model. Obrzud et al. (2009) presented a two-level parameter identification method, using the standard gradient-based optimization technique supported by the feed-forward neural network algorithm, to calibrate an elastoplastic model.

In this paper, an optimization algorithm DIRECT, developed by Finkel (2003), was adopted and integrated to constitutive model calibration. The method is a modification to Lipschitzian optimization (Perttunen 1993), which was designed to solve difficult global optimization problems with bound constraints and a real-valued objective function (Finkel, 2003).

3.2 Numerical Optimization

Optimization problems are generally defined as minimizing the objective function $f(\boldsymbol{x})$ subject to decision variable vector $\boldsymbol{x}$. Numerical optimization algorithms typically can be categorized into three groups according to the type of information needed in searching for the minimum of the objective functions. The simplest way to minimize the objective function is to randomly choose a sufficiently large number of candidate vectors **x** and evaluate the objective function for each of them. This approach is often referred to as zero-order methods, in which random search methods, like Rosenbrock method (Rosenbrock 1960), Powell's method (Powell 1964), Simplex method (Nelder and Mead 1965), and DIRECT method (Finkel 2003) are of this kind. If the information of the gradient of the objective function is implemented into the optimization algorithm, it is referred to as first-order methods. Second-order methods, also called Newton's methods, use the information of the second derivatives of the objective function (Hessian matrix H) throughout the optimization process.

Due to the nature of the incremental format of most elastoplastic constitutive drivers, the objective functions are not explicitly well-defined. This causes the difficulty in calculating the first and second derivatives of objective functions when first-order methods and second-order methods are used. Therefore, in this paper, the zero-order method, DIRECT, is used and integrated in a model calibration. The algorithm uses the information from its sampling points in the domain to decide the next search direction. It globally minimizes the objective function; however, the convergence may be computationally expensive. The detailed discussion on its algorithm can be found in Finkel (2003).

3.3 Objective Function

Since constitutive models are being calibrated, it is intuitive to use stress and strain as variables in the objective function. It is then straightforward to formulate the objective function as the sum of distances from computed points to their adjacent experimental points in the stress strain space. Figure 3.1 shows three different forms of objective function considered in this study. For Case A, the distance is computed between each laboratory data point and the corresponding numerical model point at the same stress level, however for Case B, the distance is measured between the laboratory and numerical point at the same strain level. As for Case C, the objective function is constructed in the sense of least-squares from each laboratory point to the numerical stress-strain response from a given constitutive model.

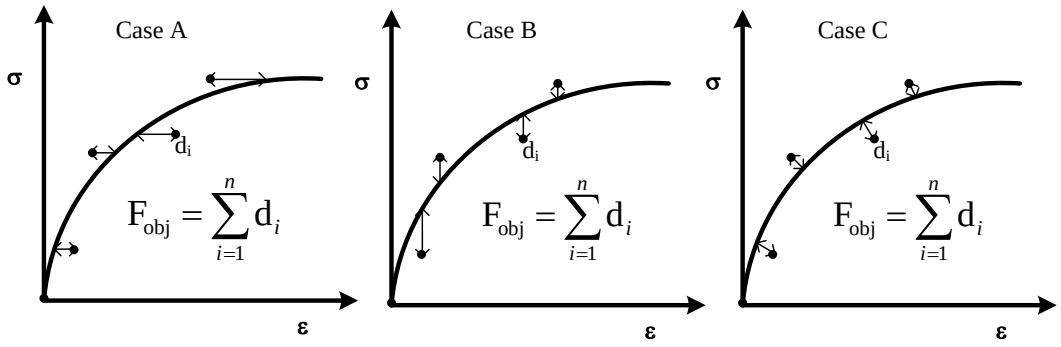

Figure 3.1 Illustration of formulating the objective function for constitutive model calibration

The modified Cam-Clay model (Muir Wood 1990) is used in this study to demonstrate the effectiveness of the proposed objective functions. Since it is a well-known constitutive model, only the essence of the model is presented here. The yield function is expressed as

$$f = q^2 + M^2 p^2 - M^2 p p_0, \tag{3.1}$$

where,

p is the effective mean stress, q is the deviatoric stress, p_0 is preconsolidation mean stress which control the initial size of the yield function, and M is the critical state slope in p-q stress space.

The associated flow rule is used to compute the incremental plastic volumetric strain $\dot{\varepsilon}_v^p$ and incremental plastic deviatoric strain $\dot{\varepsilon}_d^p$, for example

$$\dot{\varepsilon}_v^p = \Lambda \partial f / \partial p \text{ and } \dot{\varepsilon}_d^p = \Lambda \partial f / \partial q \tag{3.2}$$

where,

Λ is the incremental plastic multiplier and $\partial f / \partial p$ and $\partial f / \partial q$ are gradients of the yield function with respect to *p* and *q*.

The isotropic hardening rule is given by

$$\dot{p}_0 = p_0(1+e_0)/(\lambda-\kappa)\dot{\varepsilon}_v^p, \tag{3.3}$$

where,

e_0 is the initial void ratio; λ and κ are the slopes of compression and re-compression paths in the void ratio versus the natural logarithm of effective mean stress plot.

After applying additive strain decomposition, plastic flow rule into the consistency condition of the yield function, the incremental plastic multiplier can be determined. With that, the incremental stress-strain relation in matrix form can be expressed as

$$\begin{pmatrix} \dot{p} \\ \dot{q} \end{pmatrix} = \left\{ \begin{bmatrix} K & 0 \\ 0 & 3G \end{bmatrix} - \frac{1}{h} \begin{bmatrix} K^2M^4(2p-p_0)^2 & 6KGM^2q(2p-p_0) \\ 6KGM^2q(2p-p_0) & 36G^2q^2 \end{bmatrix} \right\} \begin{pmatrix} \dot{\varepsilon}_v \\ \dot{\varepsilon}_d \end{pmatrix}, \tag{3.4}$$

where,

$$h = KM^4(2p-p_0)^2 + 12Gq^2 + \frac{M^4pp_0(1+e_0)(2p-p_0)}{\lambda-\kappa}\ . \tag{3.5}$$

Also,

$$K = \frac{\kappa}{P_0(1+e_0)} \tag{3.6}$$

is bulk modulus and *G* is shear modulus.

3.4 Results and Discussion

There are six independent model parameters in the modified Cam-Clay model, which include λ, κ, G, M, e_0, and p_0. The drained triaxial test on remolded normally-consolidated Weald clay from Bishop and Henkel (1957) was selected in this work. Two-variable optimization analyses were first carried out using the Case A, Case B, and Case C objective functions, respectively. In this series of computation, model parameters λ and G were variables while M, e_0, k, and p_0 remained fixed. Before running the optimization, upper bound and lower bound of the variables ($0 \le \lambda \le 1$ and $3400 \le G \le 3800$) needed to be specified. Table 3.1 gives the calculated model parameters through numerical optimization. Figure 3.2 shows the stress-strain curves from the optimized modified Cam-Clay model and the data points from the laboratory test, in which good matches were generally found. Figure 3.3 displays the iteration process for each case. Since the way the objective functions were defined was different in each case, the values of the objective functions should not be used to assess their effectiveness. It is found in figure 3.3 that Case A converged rapidly after 3 iterations, while Cases B and C reached a convergent state after 10 and 12 iterations, respectively. However, it does not guarantee that Case A objective function is superior than Cases B and C. If we take a close look at figure 3.2, in comparison to Cases B and C, the stress-strain curve from the calibrated model in Case A does not show a good match around the deviatoric strain at 5%. This is probably due to the fact that Case A objective function is not sensitive to stress states where plastic deformation is more significant than elastic deformation.

Table 3.1 Optimized model parameters

Objective Function	Optimized λ	Optimized G
Case A	0.0740	3400.52
Case B	0.0689	3414.78
Case C	0.0693	3403.26

Note: M = 0.9, e_0 = 0.933, κ = 0.015, and p_0 = 207 kPa were used and kept constant during calibration.

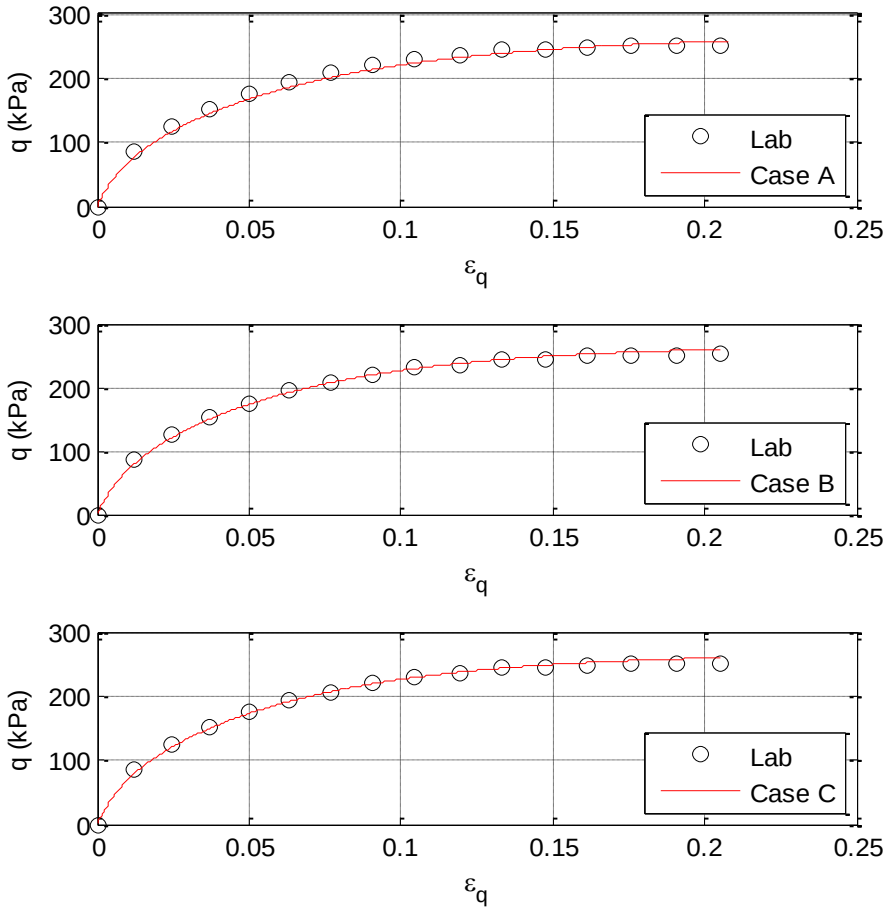

Figure 3.2 Two-variable optimization model calibrations using proposed objective functions

In the second series of computation, a further investigation on Case C objective function was performed by adding more variables in each optimization as shown in table 3.2. Again, the upper and lower bounds of the variables,

$$(0 \le \lambda \le 1,\ 3400 \le G \le 3800,\ 0.8 \le M \le 0.95, \text{ and } 0.8 \le e_0 \le 1.0) \qquad (3.7)$$

were specified.

The stress-strain curves shown in figure 3.4 correspond well when compared to the laboratory test results. Figure 3.5 shows the corresponding iteration process for each optimization. The values of the objective functions converged after 12, 10, and 14 iterations for 2, 3, and 4-variable optimizations, respectively. It also found that in the 4- variable optimization, the converged value of its objective function is greater than the ones in the 2 and 3-variable optimizations.

Table 3.2 Optimized model parameters through the Case-C objective function.

	λ	G	M	e_0	κ
2-Variable Optimization	0.0693	3403.26	N/A	N/A	N/A
3-Variable Optimization	0.0556	3402.47	0.8664	N/A	N/A
4-Variable Optimization	0.0761	3710.29	0.9133	0.9551	N/A

Note: M = 0.9, e_0 = 0.933, κ = 0.015, and p_0 = 207 kPa were used and kept constant during calibration if not being optimized.

Table 3.3 Iterations of the two-variable optimization model calibration using proposed objective functions

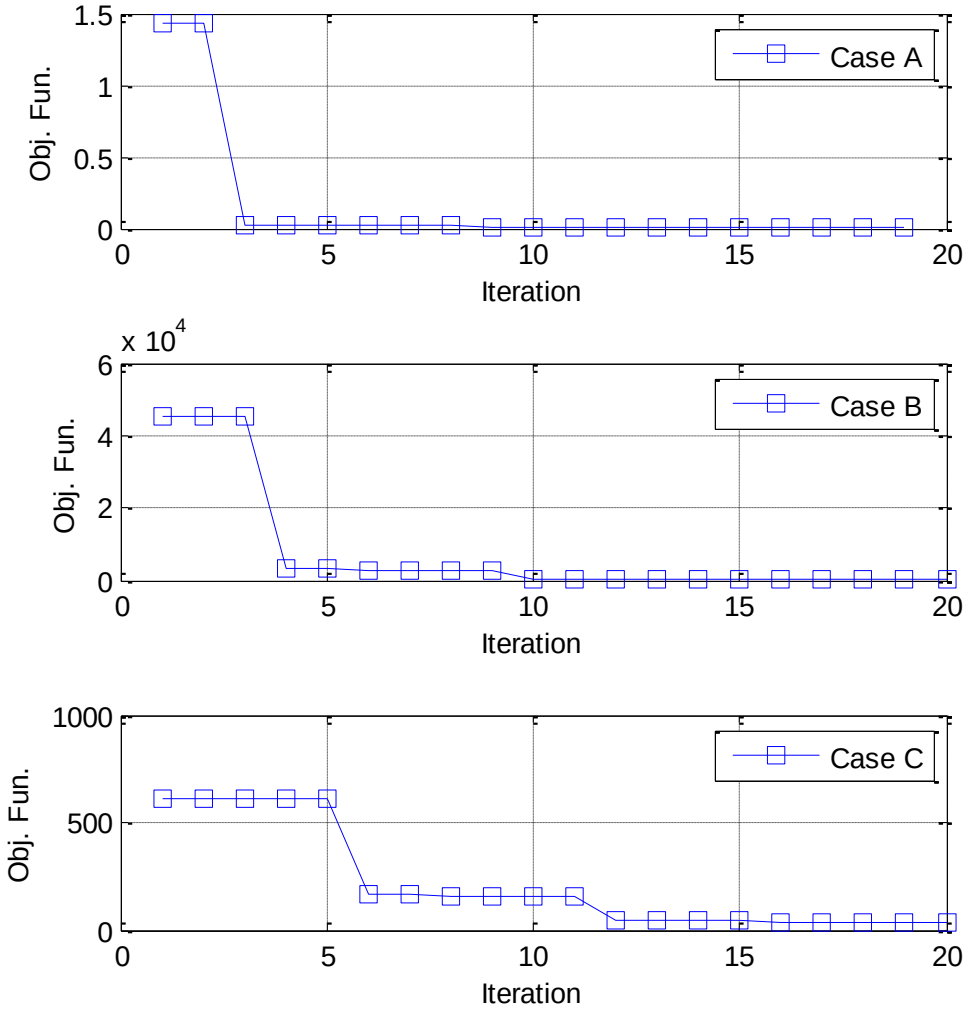

Table 3.4 Two-, three-, and four-variable optimization model calibrations using Case-C objective function

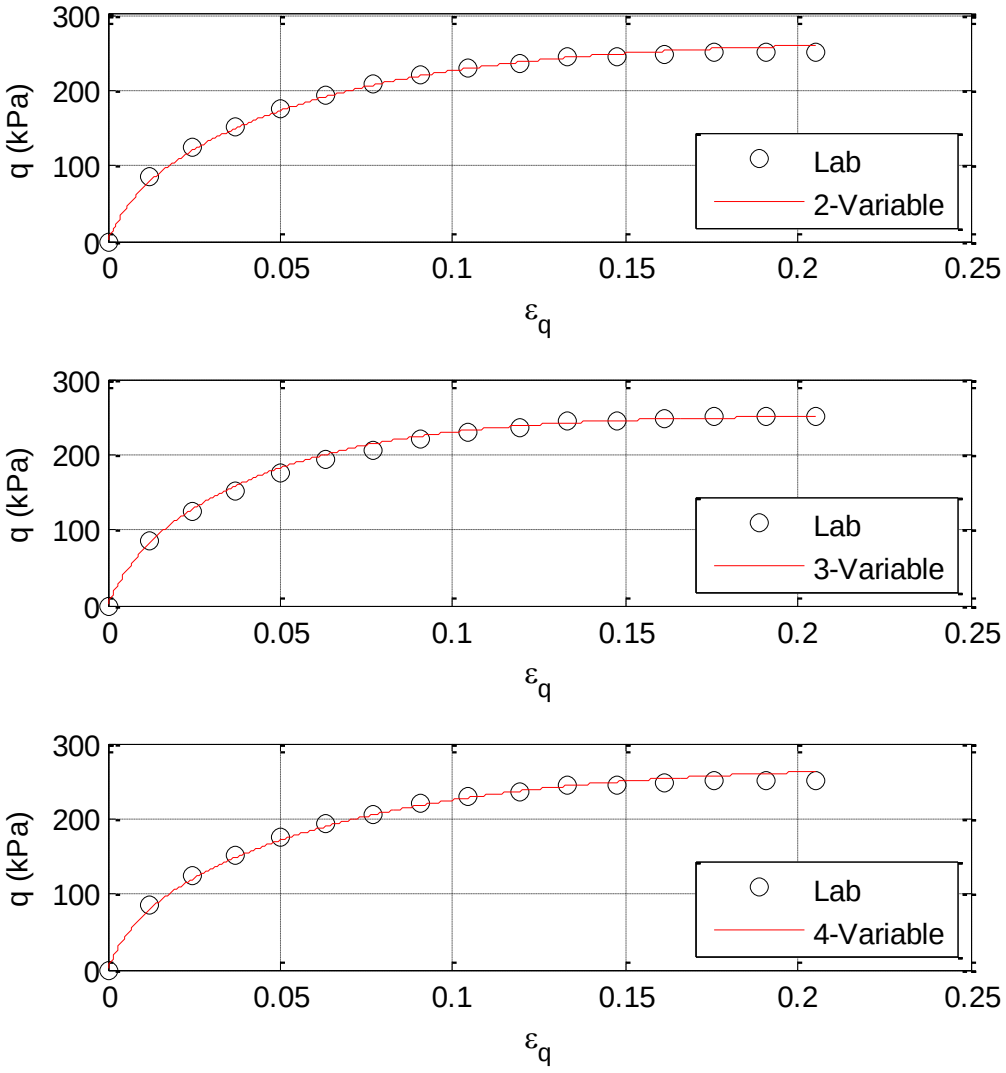

Table 3.5 Iterations of the two, three, and four-variable optimization model calibration using Case C objective function

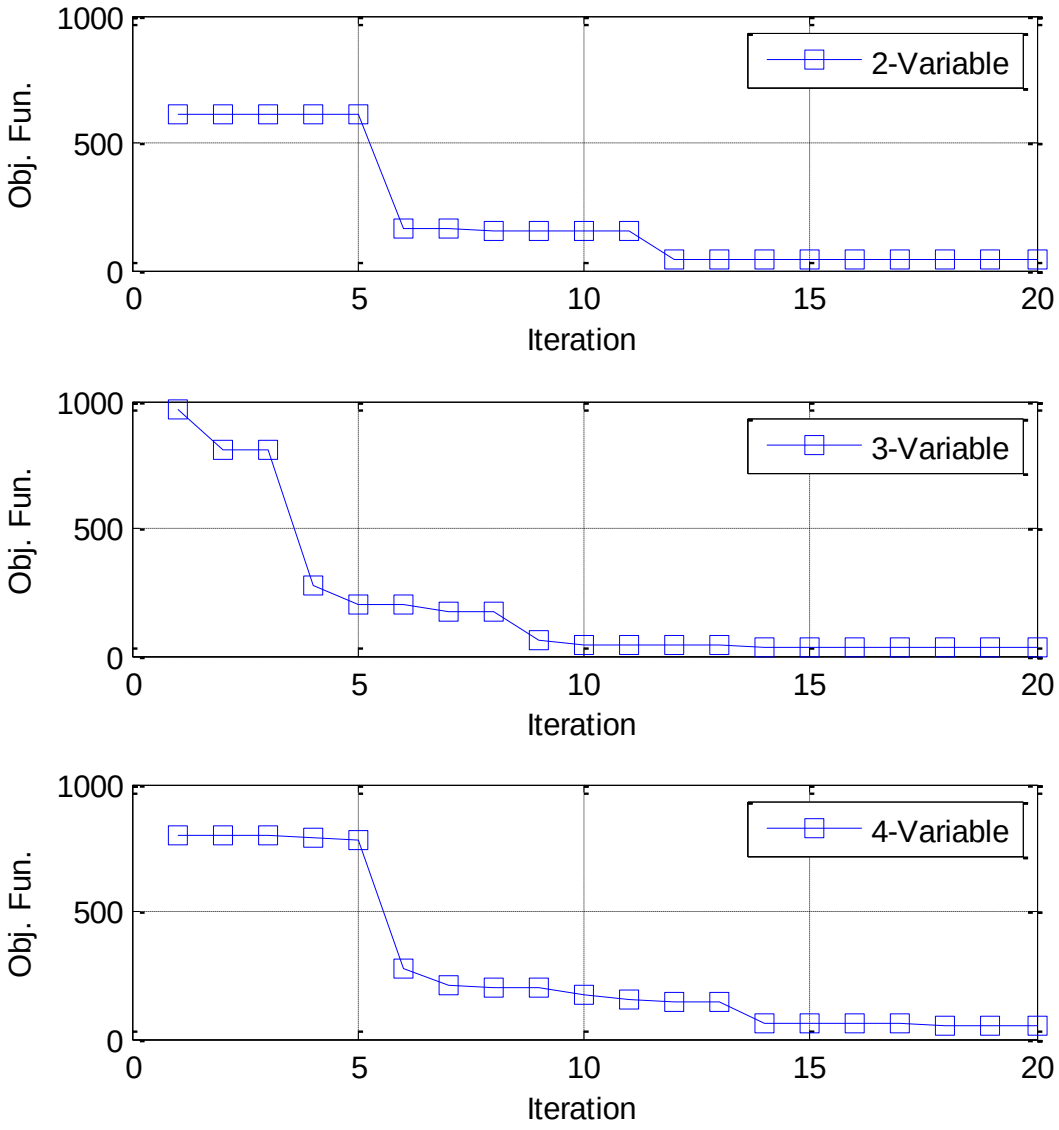

3.5 Summary

A bound unconstrained numerical optimization using DIRECT algorithm was applied to constitutive model calibration. The modified Cam-Clay model was calibrated against the laboratory test data. All of the proposed objective functions worked effectively, however the least-square type of objective function (Case C) is preferred. Up to four variables were calibrated by using the Case C objective function. As stated, upper and lower bounds of the variables to be calibrated need to be specified. The efficiency of the optimization relies on the determination of the bound values. It is suggested that the optimization technique be used when fine-tuning a constitutive model rather than as a preliminary calibration.

References

Anandarajah, A. 1994. A granular material model based on associated flow rule applied to monotonic loading behavior. *Soils and Foundations* 34(3): 81-98.

Arduino, P., and E.J. Macari. 2001. Implementation of porous media formulation for geomaterials. *Journal of Engineering Mechanics* 127(2): 157-166.

Bardet, J.P. 1985. Bounding surface plasticity model for sands. *Journal of Engineering Mechanics* 112(11): 1198-1217.

Bishop, A.W., and D.J. Henkel. 1957. *The measurement of soil properties in the triaxial test*. London: E. Arnold Publication.

Calvello, M. and R.J. Finno. 2004. Selecting parameters to optimize in model calibration by inverse analysis. *Computers and Geotechnics* 31: 411-425.

Cekerevac, C., S. Girardin, G. Klubertanz, and L. Laloui. 2006. Calibration of an elasto-plastic constitutive model by constrained optimization procedure. *Computers and Geotechnics* 33: 432-443.

Chazallon, C., P. Hornych, and S. Mouhoubi. 2006. Elastoplastic model for long-term behavior modeling of unbound granular materials in flexible pavements. *International Journal of Geomechanics* 6(4): 279-289.

Finkel, D.E. 2003. DIRECT Optimization Algorithm User Guide, Center for Research in Scientific Computation, North Carolina State University, Raleigh, NC. http://www4.ncsu.edu/~ctk/Finkel_Direct/.

Gajo, A., and D. Muir Wood. 1999. A kinematic hardening constitutive model for sands: The multiaxial formulation. *International Journal for Numerical and Analytical Methods in Geomechanics* 23: 925-965.

Garcia-Rojo, R., and H.J. Herrmann. 2005. Shakedown of unbound granular material. *Granular Matter* 7: 109-118.

Ge, Y.-N. 2003. Cyclic Constitutive Modeling of Granular Materials. PhD Diss., University of Colorado at Boulder.

Ge, Y.-N., and S. Sture. 2003. Cyclic constitutive model based on fuzzy sets concepts. In *Constitutive Modeling of Geomaterials*, ed. H.I. Ling, A. Anandarajah, M.T. Manzari, V. N. Kaliakin, and A. Smyth, 108-112. CRC Press.

Ge, Y.-N., and S. Sture. 2003. Integration and application of a cyclic plasticity model for geomaterials. In *Proceedings of the 16th ASCE Engineering Mechanics Division Conference.* Seattle, WA.

Jacobsson, L. and K. Runnesson. 2002. Integration and calibration of a plasticity model for granular materials. *International Journal for Numerical and Analytical Methods in Geomechanics* 26: 259-272.

Johansson, H. and K. Runnesson. 2005. Parameter identification in constitutive models via optimization with a posteriori error control. *International Journal for Numerical Methods in Engineering* 62: 1315-1340.

Johnson, D., and B. Sukumaran. 2009. Investigation of the performance of flexible airport pavements under moving aircraft wheel loads with wander using finite element analysis. In *Soils and Rock Instrumentation, Behavior and Modeling*, Geotechnical Special Publication No. 194, ed L. Ge, B. Tang, W. Wei, and R. Chen, 44-49. Reston, VA: American Society of Civil Engineers.

Kim, M., and E. Tutumluer. 2008. Multiple wheel-load interaction in flexible pavements. *Transportation Research Record* 2068: 49-60.

Klisinski, M. 1991. Plasticity theory based on fuzzy sets. *Journal of Engineering Mechanics* 114(4): 563-582.

Klisinski, M., N. Abifadel, K. Runesson, and S. Sture. 1991. Modeling of the behavior of dry sand by an elasto-plastic "fuzzy set" model. *Computers and Geotechnics* 11: 229-261.

Klisinski, M., M.M. Alawi, S. Sture, H.-Y. Ko, and D. Muir Wood. 1988. Elasto-plastic model for sand based on fuzzy sets. In *Constitutive Equations for Granular Non-cohesive Soils*, ed. G.F. Bianchini and A.S. Saada. Rotterdam, Netherlands: Taylor & Francis.

Lekarp, F. 1997. Permanent deformation behaviour of unbound granular meterials. Licentiate thesis, KTH, Sweden.

Lekarp, F., U. Isacsson, and A. Dawson. 2000a. "State of the art Ⅱ: Permanent strain response of unbound aggregates. *Journal of Transportation Engineering* 126(1): 76-83.

Lekarp, F., U. Isacsson, and A. Dawson. 2000b. State of the art I: Resilient response of unbound aggregates. *Journal of Transportation Engineering* 126(1): 66-75.

Manzari, M. T., and Y.F. Dafalias. 1997. A critical state two-surface plasticity model for sands. *Géotechnique* 47(2): 335-339.

Mattsson, H., M. Klisinski, and K. Axelsson. 2001. Optimization routine for identification of model parameters in soil plasticity. *International Journal for Numerical and Analytical Methods in Geomechanics* 25: 435-472.

Mróz, Z., V.A. Norris, and O.C. Zienkiewicz. 1978. An anisotropic hardening model for soils and its application to cyclic loading. *International Journal for Numerical and Analytical Methods in Geomechanics* 2: 203-221.

Muir Wood, D. 1990. *Soil Behaviour and Critical State Soil Mechanics*. Cambridge, MA: Cambridge University Press.

Muir Wood, D., K. Belkheir, and D.F. Liu. 1994. Strain softening and state parameter for sand modeling. *Géotechnique* 44(2): 335-339.

Nelder, J.A. and R.A. Mead. 1965. A simple method for function minimization. *The Computer Journal* 7: 308-313.

Nova, R., and D.M. Wood. 1979. A constitutive model for sand. *International Journal for Numerical and Analytical Methods in Geomechanics* 3(3): 255-278.

Obrzud, R., L. Vulliet, and A. Truty. 2009. Optimization framework for calibration of constitutive models enhanced by neural networks. *International Journal for Numerical and Analytical Methods in Geomechanics* 33: 71-94.

Pastor, M., and O.C. Zienkicwcz. 1986. A generalized plasticity hierarchical model for sand under monotonic and cyclic loading. In *NUMOG II Conference Proceeding*, ed. G. Ghent, N. Pande, and W.F. Van, 131-150.

Perttunen, C.D., D.R. Jones, and B.E. Stuckman. 1993. Lipschitzian optimization without the lipschitz constant. *Journal of Optimization Theory and Application* 79(1): 157-181.

Powell, M.J.D. 1964. An efficient method of finding the minimum of a function of several variables without calculating derivatives. *The Computer Journal* 7: 155-162.

Pradhan, T.B.S., F. Tatsuoka, and Y. Sato. 1989. Experimental stress-dilatancy relations of sand subjected to cyclic loading. *Soils and Foundations* 29(1): 45-64.

Prévost, J.H. 1978. Plasticity theory for soil stress behavior. *Journal of Engineering Mechanics* 104(5): 1177-1194.

Prévost, J. H. 1982. Two surface versus multi-surface plasticity theories: A critical assessment. *International Journal for Numerical and Analytical Methods in Geomechanics*. 6(3): 323-338.

Rosenbrock, H.H. 1960. An automatic method for finding the greatest or least value of a function. *The Computer Journal* 3: 175-184.

Samarajiva, P., E.J. Macari, and W. Wathugala. 2005. Genetic algorithms for calibration of constitutive models for soils. *International Journal of Geomechanics* 5(3): 206-217.

Sture, S., J.C. Mould, and H.-Y. Ko. 1982. Modeling of elastic-plastic anisotropic hardening constitutive model and prediction of behavior of dry quartz sand. In *Constitutive Relations for Soils*, ed. G. Gudenhus, F. Darve, and I. Vardoulakis, 227-248. Rotterdam, Netherlands: A. A. Balkema.

Tatsuoka, F., and K. Ishihara. 1974. Drained deformation of sand under cyclic stresses reversing direction. *Soils and Foundations* 14(3): 51-65.

Vermeer, P.A. 1982. A five-constant model unifying well-established concepts, . In *Constitutive Relations for Soils*, ed. G. Gudenhus, F. Darve, and I. Vardoulakis, 175-198. Rotterdam, Netherlands: A. A. Balkema.

Werkmeister, S., A.R. Dawson, and F. Wellner. 2004. Pavement design model for unbound granular materials. *Journal of Transportation Engineering* 130(5): 665-674.

Willam, K. J., and E.P. Warnke. 1974. Constitutive model for the triaxial behavior of concrete. In *Seminar on Concrete Structures Subjected to Triaxial Stress,* ISMES, Bergamo, Italy.

Yang, Z. and A. Elgamal. 2003. Application of unconstrained optimization and sensitivity analysis to calibration of a soil constitutive model. *International Journal for Numerical and Analytical Methods in Geomechanics* 27: 1277-1297.